Check for updates

Stable synthesis mechanism and photocatalytic properties of TiO₂ nanocrystals with different morphologies derived from potassium titanate nanowires†

Meng Chai,[ab] Bo Yuan,[c] Yao Ban,[d] Jing Guo, [ID] *[ab] Huifang Lou,[ab] Hongyuan Kang,[ab] Qiaoling Zhang,[ab] Zhiwei Liu[ab] and Dongming Zhang [ID] [ab]

This study explored key factors influencing TiO₂ morphology using potassium titanate nanowires (KTNWs) as precursors. The pH of the hydrothermal solution was identified as critical in controlling TiO₂ morphology. Different washing methods for precursors synthesized under alkaline conditions lead to varying pH environments in the subsequent hydrothermal solutions, thereby influencing the growth direction of TiO₂ nuclei. Even a very slight pH change could cause a huge difference in the morphology of TiO₂, by adjusting precursor washing methods, rod-like, cuboidal, and octahedral bipyramidal TiO₂ nanocrystals were synthesized, the octahedral bipyramidal TiO₂ exhibiting the smallest particle size. Acid treatment could stabilize the octahedral bipyramidal morphology of the TiO₂ nanocrystal, and reduced particle size by nearly 86% than that of rod-like TiO₂-R nanocrystal. Acid treated sample TiO₂-R-H7 achieved the best photocatalytic activity, which was nearly 3 times than that of original TiO₂. Adjusting $(NH_4)_2CO_3$ morphology-controlling agent concentrations further regulated {001} facet exposure ratio to improve the photocatalytic activity, the TiO₂-R-0.14 synthesized at 0.14 mmol per L $(NH_4)_2CO_3$ showing about 2.6 times than that of original TiO₂. However, excessive $(NH_4)_2CO_3$ concentrations would reduce the photocatalytic activity due to increased particle size and fewer oxygen vacancies. This study provides insights into the growth mechanisms of TiO₂ morphologies and highlights acid treatment as a strategy to reduce particle size and enhance photocatalytic activity, offering guidance for designing high-performance TiO₂ based photocatalyst.

1. Introduction

Photocatalytic technology is extensively utilized in air purification, water treatment, and sterilization, offering an effective approach to mitigating environmental pollution. TiO₂ has become one of the most widely used photocatalysts, due to its non-toxic, chemical stability, low cost, and strong photocatalytic activity. However, the wide bandgap of TiO₂ and the rapid recombination of photo-generated electron–hole pairs restrict it to UV light excitation and result in low quantum efficiency, limiting its industrial applications.[1] To address these limitations, TiO₂ is commonly modified by methods such as ion doping, noble metal loading, semiconductor coupling, and facet engineering to enhance its photocatalytic efficiency.[2,3] Among them, facet engineering normally using morphology-controlling agents to expose the high-energy crystal face of TiO₂ to improve its photocatalytic activity. Furthermore, the heterojunction between the {001} and {101} facets can promote the migration and separation of photo-generated electron–hole pairs, further improving the photocatalytic activity of TiO₂.[4] However, following the principle of the lowest surface energy, TiO₂ crystals will spontaneously expose the low-energy {101} crystal face with an energy of 0.44 J m⁻² under natural conditions.[5] To expose the high-energy {001} crystal face (0.90 J m⁻²), facet-controlling agents are needed to reduce its surface energy.[6,7] Due to the slow hydrolysis rate of titanate nanowires, which is beneficial to the selective adsorption of morphology-controlling agents onto the {001} crystal face, many researchers choose titanate nanowires ($K_2Ti_3O_7$ or $Na_2Ti_3O_7$) as the precursor for morphology-controlled TiO₂ synthesis.[8,9] $(NH_4)_2CO_3$ is inexpensive and readily available, can reduce the surface energy of the {001} facet, and the NH_4^+ can act as a pH buffer, providing a stable environment for TiO₂ crystal growth.[10] Therefore, this study employs $(NH_4)_2CO_3$ as the morphology-controlling agent.

[a]*Shanxi Province Key Laboratory of Chemical Process Intensification, School of Chemistry and Chemical Engineering, North University of China, Taiyuan 030051, China. E-mail: guojing0519@nuc.edu.cn*

[b]*State Key Laboratory of Coal and CBM Co-Mining, North University of China, Taiyuan 030051, China*

[c]*Ordos Carbon Neutral Research and Application Co., Ltd, Ordos 017010, China*

[d]*Sinopec Maoming Company, Maoming 525099, China*

† Electronic supplementary information (ESI) available. See DOI: https://doi.org/10.1039/d4ra08805k

The photocatalytic activity of the photocatalyst is not only related to the exposure of the crystal facet, but also related to its specific surface area. Previous studies have shown that acid treatment of titanates can reduce the particle size of hydrothermally synthesized TiO_2 nanocrystals, increase their specific surface area, and thereby enhance their photocatalytic activity. Chacko et al. employed an alkaline hydrothermal method to convert TiO_2 into potassium titanate nanowires, which was then subjected to acid treatment and ion exchange to form a titanate precursor ($H_2Ti_3O_7$). Subsequent hydrothermal treatment yielded ultrafine TiO_2 nanofibers. BET analysis revealed that the modified TiO_2 had a specific surface area 2.5 times that of the pristine TiO_2.[11] Viet et al. conducted sodium titanate to water washing and acid treatment for 30 minutes, followed by hydrothermal treatment at 135 °C for 24 hours. The results showed that water washing produced irregular TiO_2 nanoblocks with a particle size of approximately 38 nm, while acid treatment yielded TiO_2 nanotubes with a diameter of about 10 nm and a specific surface area 2.03 times that of the original TiO_2.[12] Furthermore, acid treatment can reduce alkali metal ions in titanates and thereby modifying the morphology and particle size of hydrothermally synthesized TiO_2. Xiong et al. treated sodium titanate nanowires with HNO_3 at various concentrations for 6 hours. After acid treatment, the precursor was subjected to hydrothermal processing at 180 °C for 24 hours, the specific surface area of the produced TiO_2 was 1.9 times that of the TiO_2 synthesized without precursor acid treatment. The photocatalytic degradation efficiency of this TiO_2 for MO was twice that of commercial P25. This acid treatment reduced the Na^+ content in the precursor from 7.37% to zero, resulting in a morphological transition of the synthesized TiO_2 from rod-shaped to spherical, indicating that its morphology is significantly influenced by alkali metal ions of the precursor.[13] Wei et al. utilized potassium titanate nanowires as a precursor, conducting microwave-assisted hydrothermal treatment at 160 °C for 6 hours, resulting in octahedral bipyramidal TiO_2 nanocrystals with a particle size of 17.2 nm. When using acid-treated potassium titanate nanowires as the precursor, hydrothermal synthesis similarly yielded octahedral bipyramidal TiO_2 with a particle size of approximately 16.24 nm.[14,15] It has been observed that, after acid treatment of titanate nanowires, the morphology of TiO_2 obtained through hydrothermal synthesis varies among different studies. Some researchers claimed that alkali metal ion content influences TiO_2 morphology, while other experimental results show no significant effect. Therefore, it is necessary to investigate whether the alkali metal ion content in the precursor is a primary factor affecting the morphology of synthesized TiO_2.

Studies have also indicated that the pH of the hydrothermal solution can influence the morphology of TiO_2. Du et al. treated potassium titanate nanowires with HCl, subsequently adjusting the pH of the hydrothermal solution with HCl and tetramethylammonium hydroxide at a hydrothermal temperature of 180 °C. When pH ≤ 3, rod-like TiO_2 crystals with {111} facets, approximately 90 nm in length and 20 nm in width, were synthesized. At pH 5, octahedral bipyramidal TiO_2 crystals with {010} facets and a particle size of 50 nm were obtained. When pH was between 7

and 14, spindle-shaped TiO_2 nanocrystals, approximately 200 nm in length and 30 nm in width, with exposed {001} facets were produced.[16] Wei et al. used titanates as precursors, performing microwave-assisted hydrothermal synthesis of TiO_2 at 160 °C for 6 hours under pH values of 3, 6, and 11. The results showed that in both acidic and neutral environments, bipyramidal TiO_2 nanocrystals of approximately 30 nm were synthesized, the particle size in neutral condition was slightly larger than acidic condition. When KOH was added to adjust the pH to 11, rod-like TiO_2 nanocrystals approximately 80 nm in length were obtained.[14] Chen et al. performed hydrothermal synthesis of TiO_2 nanocrystals at 175 °C after acid treatment of titanates. At pH 3.5, they obtained tetragonal TiO_2 nanocrystals with {101} facets and a particle size of 20 nm; at pH 11.5, they synthesized prismatic TiO_2 nanocrystals with {100} facets, 150 nm in length and 30 nm in width; when the pH was raised to 13.5, irregular sheet-like TiO_2 nanocrystals with {101} facets were obtained.[17] The above studies indicate that the pH of the solution significantly impacts the morphology of TiO_2 nanocrystals synthesized hydrothermally from titanate precursors. However, TiO_2 nanocrystals synthesized by different researchers under similar hydrothermal temperatures and comparable pH conditions exhibit notable differences in morphology and particle size. Our previous work also revealed significant morphological differences in TiO_2 nanocrystals synthesized in different batches under identical conditions. Therefore, when synthesizing TiO_2 nanocrystals from $K_2Ti_3O_7$ nanowires as a precursor, it is evident that factors such as hydrothermal pH, temperature and time, acid treatment of the precursor or not play crucial roles. Thus, it is essential to investigate the key factors affecting the morphology of TiO_2 nanocrystals under controlled reactant concentration, hydrothermal temperature, and reaction time. This approach will enable the controlled synthesis of TiO_2 nanocrystals, ensure batch-to-batch stability of photocatalysts, and allow facet engineering to further enhance the photocatalytic activity of TiO_2 nanocrystals.

In summary, this study investigates the effect of the pH of the hydrothermal solution on the morphology of TiO_2 nanocrystals by controlling the washing method of $K_2Ti_3O_7$ nanowire precursors. The K^+ content in $K_2Ti_3O_7$ is regulated by controlling the acid treatment duration of $K_2Ti_3O_7$ nanowires to explore the primary factors influencing the morphology and particle size of the synthesized TiO_2. Based on stable TiO_2 morphology synthesis, $K_2Ti_3O_7$ nanowires treated under optimal acid conditions are used as precursors, and a series of TiO_2 nanocrystals with varied {001} facet exposure ratios are synthesized by altering the concentration of $(NH_4)_2CO_3$ as a morphology-controlling agent. The photocatalytic degradation performance of these nanocrystals is evaluated using methylene blue as the target pollutant, aiming to produce TiO_2 nanocrystals with controlled morphology and enhanced photocatalytic activity and to provide insights for the preparation of high-activity photocatalysts.

2. Experimental

2.1 Preparation of potassium titanate nanowires

A total of 1.0 g of anatase TiO_2 nanoparticles with a particle size of 20 nm was weighed and dispersed in 70 mL of 10 mol per L

KOH solution. The mixture was subjected to ultrasonic treatment for 30 minutes to form a homogeneous white suspension. Subsequently, the suspension was transferred to a Teflon-lined stainless-steel autoclave for hydrothermal treatment at 180 °C for 16 hours. After the reaction, the autoclave was allowed to cool naturally to room temperature inside the oven. The reaction products were washed thoroughly using deionized water or a combination of acid washing followed by water washing to remove impurities. The washed products were separated *via* centrifugation and then dried to obtain the potassium titanate nanowire precursor (KTNWs). The synthesized potassium titanate nanowires were designated as R-KTNWs.

2.2 Potassium titanate nanowires acid treatment

1.0 g R-KTNWs precursor was added to 60 mL of 1 mol per L HCl solution. The mixture was stirred for varying durations, followed by centrifugation to separate the solid product. The separated product was washed repeatedly with deionized water until the washing solution reached neutral pH. After the final centrifugation, the product was dried and collected for further use.

2.3 Preparation of TiO$_2$ nanocrystals

A total of 0.1 g of R-KTNWs was dispersed in 70 mL of deionized water and subjected to ultrasonic treatment to ensure uniform dispersion. The resulting suspension was transferred into a Teflon-lined stainless-steel autoclave and subjected to hydrothermal treatment at 180 °C for 16 hours. After the reaction, the autoclave was allowed to cool naturally to room temperature in the oven. The products were washed repeatedly with deionized water until the supernatant reached a neutral pH. Finally, the products were dried to obtain the series of TiO$_2$ nanocrystals.

The preparation conditions are summarized in Table 1. Specifically, the sample labeled as TiO$_2$-R refers to TiO$_2$ obtained from R-KTNWs without acid treatment, while TiO$_2$-R-H0 denotes TiO$_2$ nanocrystals prepared *via* hydrothermal treatment following HCl solution washing. For samples labeled as TiO$_2$-R-HX, the value of X represents the duration of acid treatment in hours.

2.4 Preparation of TiO$_2$ nanocrystals with exposed {001} facets

0.1 g R-KTNWs precursor was added to (NH$_4$)$_2$CO$_3$ solutions of varying concentrations. The mixture was ultrasonically

dispersed to form a homogeneous suspension, which was then transferred to a Teflon-lined stainless-steel autoclave for hydrothermal treatment at 180 °C for 16 hours. After the reaction, the product was separated *via* centrifugation and washed thoroughly with distilled water until the supernatant became neutral. The washed product was subsequently dried for further analysis. The detailed preparation conditions are summarized in Table 2. In the sample notation TiO$_2$-R-H7-Y, Y denotes the concentration of (NH$_4$)$_2$CO$_3$ in the solution.

2.5 Characterization

Scanning electron microscopy (SEM, SIGMA500, Germany) and transmission electron microscopy (TEM, Talos F200S, G2, America) were used to observe the microscopic morphology of the samples. The light absorption capacity of the samples was analyzed and measured using a UV-visible spectrometer (Agilent Carry5000, America) with BaSO$_4$ as the reference and a scanning wavelength range of 200–800 nm. The steady-state photoluminescence (PL) spectra were recorded using an FL fluorescence spectrophotometer (F-7000, Japan) with a stimulating wavelength range of 260 nm. The paramagnetic resonance spectrometer (EPR, Bruker MS 5000X, Germany) was used to test the active substances of the samples. The crystal structure of TiO$_2$ catalyst was determined by X-ray diffractometer (XRD, D8 Advance). The scanning range was $2\theta = 20$–$80°$, the scanning speed was $10°$ min^{-1}, the step size was $0.02°$, the X-ray source was Cu Kα, the tube voltage was 40 kV, and the tube current was 100 mA.

2.6 Photocatalytic evaluation

The photocatalytic degradation of methylene blue (MB) dye was investigated under a 15 W, 365 nm UV lamp to evaluate the photocatalytic activity of the series of photocatalysts. A total of 30 mg of TiO$_2$ catalyst was added to 30 mL of 10 mg per L MB solution. The mixture was stirred in the dark for 30 min to achieve adsorption–desorption equilibrium. After centrifugation, the supernatant was collected, and its absorbance at 664 nm was measured and recorded as A_0. Subsequently, samples were taken at regular intervals during UV irradiation, and the corresponding absorbance values were measured and recorded as A_i. The degradation rate of the MB dye under UV irradiation was calculated using eqn (1).

$$\eta = \frac{A_0 - A_i}{A_0} \times 100\% \qquad (1)$$

At low dye concentrations, the TiO$_2$ photocatalytic reaction follows pseudo-first-order kinetics. The degradation kinetics were fitted using eqn (2), expressed as:

$$\ln(c_t/c_0) = -k_{app}t \qquad (2)$$

where t represents the reaction time, k_{app} is the apparent rate constant, and c_0 and c_t are the pollutant concentrations at $t = 0$ and $t = t$, respectively.

Table 1 Synthesis conditions of acid-treated TiO$_2$ nanocrystals

R-KTNWs/g	H$_2$O/mL	Acid treatment time/h	Named
0.1	70	—	TiO$_2$-R
0.1	70	Washing	TiO$_2$-R-H0
0.1	70	7	TiO$_2$-R-H7
0.1	70	24	TiO$_2$-R-H24
0.1	70	48	TiO$_2$-R-H48

Table 2 Synthesis conditions of TiO_2 nanocrystals with exposed {001} facets

R-KTNWs/g	H_2O/L	$(NH_4)_2CO_3$/mmol L^{-1}	Acid treatment time/h	Named
0.1	70	0	0	TiO_2-R
0.1	70	0.07	0	TiO_2-R-0.07
0.1	70	0.14	0	TiO_2-R-0.14
0.1	70	0.28	0	TiO_2-R-0.28
0.1	70	0	7	TiO_2-R-H7
0.1	70	0.07	7	TiO_2-R-H7-0.07
0.1	70	0.14	7	TiO_2-R-H7-0.14

3. Results and discussion

3.1 Effect of pH on the morphology of TiO_2 nanocrystals

3.1.1 Morphology of TiO_2 nanocrystals under different synthesis conditions. Fig. 1(a) presents the SEM image of potassium titanate nanowires (R-KTNWs) synthesized *via* hydrothermal treatment of anatase TiO_2 nanoparticles in KOH solution. During the reaction, TiO_2 nanoparticles undergo hydrolysis in KOH solution to form amorphous $Ti(OH)_4$, whose octahedral units connect *via* edge-sharing to establish a framework. K^+ associate with the $Ti(OH)_4$ structure through electrostatic interactions. Over time, under high-temperature and high-pressure conditions, a fibrous network structure emerges, eventually forming R-KTNWs, as shown in Fig. 1(a).

Using the R-KTNWs as precursors, further hydrothermal treatment can produce a series of TiO_2 nanocrystals. Analysis of experimental results from different batches indicates that, under constant reactant concentration, hydrothermal temperature, and reaction time, the surface properties of the potassium titanate precursor are likely the critical factors determining the final morphology of the TiO_2 nanocrystals. The transformation of commercial TiO_2 to R-KTNWs occurs in a strongly alkaline environment. Achieving a completely neutral product through simple deionized water washing is challenging. Although washing steps were standardized, variations in water volume and washing duration affected the thoroughness of precursor washing. Differences in the washing degree of R-KTNWs result in varying pH of the subsequent hydrothermal solution, potentially influencing the morphology of the synthesized TiO_2 nanocrystals.

To validate this hypothesis, a series of experiments were conducted. R-KTNWs were prepared hydrothermally using anatase TiO_2 nanoparticles as the raw material. The nanowires were then subjected to different washing treatments, including acid washing followed by deionized water washing to subacidity, repeated deionized water washing to slight alkalinity, and deionized water washing resulting in weakly alkaline conditions. The treated precursors were hydrothermally processed at 180 °C for 16 h to produce TiO_2 nanocrystals, with their morphologies characterized *via* SEM, as shown in Fig. 1(b–d). Fig. 1(b) demonstrates that TiO_2-R-H0 nanocrystals with a bipyramidal morphology and an average particle size of approximately 52 nm were obtained when the R-KTNWs were acid-washed and then washed with water to subacidity. In
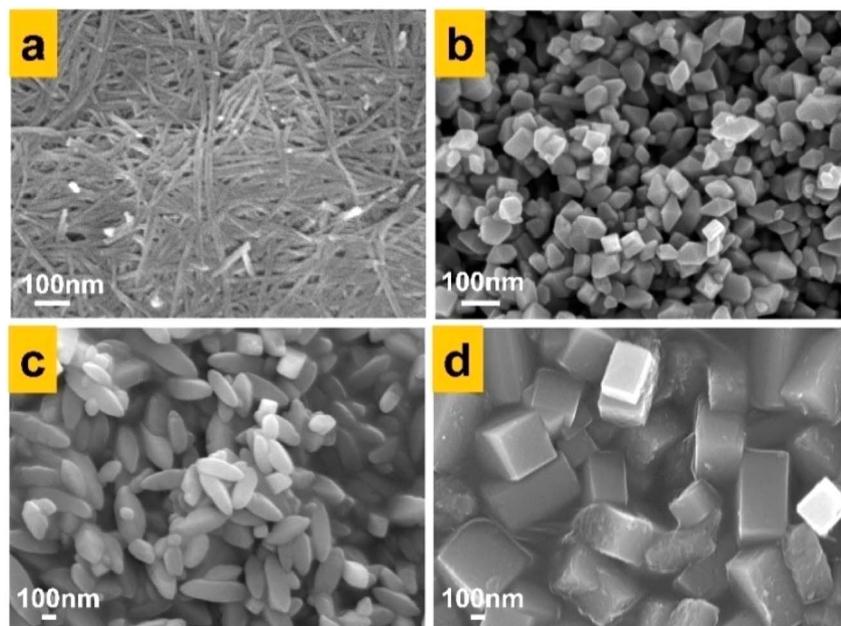

Fig. 1 SEM images of KTNWs precursor and TiO_2 nanocrystals with different morphologies (a) R-KTNWs, (b) TiO_2-R-H0, (c) TiO_2-R, (d) TiO_2-R-alk.
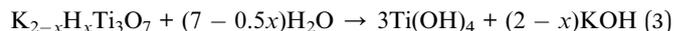
contrast, washing the nanowires only with deionized water to slight alkalinity yielded rod-like TiO_2 nanocrystals under identical conditions, named TiO_2-R (Fig. 1(c)), with an average width of ~103 nm and length of ~303 nm. When the R-KTNWs were insufficiently washed and remained weakly alkaline, the hydrothermal process resulted in cuboidal TiO_2 nanocrystals, named TiO_2-R-alk, as shown in Fig. 1(d), with dimensions of ~384 nm in length and ~228 nm in width. As show in Fig. 2, the high-resolution transmission electron microscopy (HRTEM) revealed that the lattice fringes of the TiO_2 with the three different morphologies exhibited a spacing of 0.35 nm, corresponding to the {101} crystal plane, which is the most stable facet under natural conditions.

The results demonstrate that the washing method of R-KTNWs precursors indirectly regulates the pH environment of the subsequent hydrothermal solution. Acid washing followed by water rinsing produces a slightly acidic solution, extensive repeated water washing results in a slightly alkaline solution, and insufficient washing leads to a more alkaline solution. These variations in the hydrothermal pH environment ultimately result in TiO_2 nanocrystals with different morphologies. Although the pH of the final solution through the above three washing methods is close to 7, subtle changes in the pH of the hydrothermal solution played a critical role in controlling the morphology of TiO_2 nanocrystals. Additionally, as the pH of the solution increases, the particle size of TiO_2 nanocrystals also increases. TiO_2 nanocrystals obtained from acid-washed R-KTNWs precursors exhibit smaller particle sizes and larger specific surface areas, which are more advantageous for enhancing photocatalytic activity.

3.1.2 The growth mechanism of different TiO_2 morphologies. Based on SEM morphology and reaction mechanisms, the possible growth mechanisms of TiO_2 nanocrystals with the three distinct morphologies under different pH environments were analyze and illustrated in Fig. 3. The transformation of R-KTNWs into TiO_2 nanocrystals follows a "dissolution–recrystallization" nucleation mechanism. Under hydrothermal conditions, the R-KTNWs gradually decompose into $Ti(OH)_4$ fragments, –OH groups, and K^+ ions, as described in eqn (3), this stage represents the hydrolysis process. Subsequently, $Ti(OH)_4$ fragments undergo rearrangement via dehydration reactions between Ti–OH and HO–Ti groups, forming octahedral TiO_2 crystal nucleus through edge-sharing, as shown in eqn (4), this stage corresponds to the condensation process.[18] Later on, the TiO_2 crystal nucleus gradually grow up to form

nanocrystalline TiO_2 when $Ti(OH)_4$ fragments diffused to their surface.

$$K_{2-x}H_xTi_3O_7 + (7 - 0.5x)H_2O \rightarrow 3Ti(OH)_4 + (2 - x)KOH \quad (3)$$

$$Ti(OH)_4 \rightarrow TiO_2 + 2H_2O \quad (4)$$

Because of the anisotropy in adsorption stability of the capping agents, the adsorbates adsorbed onto specific crystallographic faces more strongly than others. This reduces the surface energy of the bound facet and hinders the growth of crystals or some crystal facets. Barnard et al. investigated the surface structures and energies of selected low-index surfaces for both rutile and anatase forms of TiO_2. They discovered that under basic conditions, the oxygen-terminated {100} facets exhibit lower surface energy compared to the oxygen-terminated {101} and {001} facets.[19,20] Yu et al. also believed that the OH^-, which are gradually released from Na-titanate nanotubes, would preferentially attach to the anatase {100} facets. This selective adsorption lowers the surface energy of the {100} facets, thereby restricting the crystal growth along the a- and b-axes, the concentration of OH^- would gradually decrease with the reaction, resulting in spindle or round-rod shapes.[18]

As illustrated in Fig. 3, in the present system, R-KTNWs with deionized water washing resulting in weakly alkaline conditions, we consider that the following hydrothermal reaction at a fixed basic condition, the selective adsorption of OH^- would lower the surface energy of the {100} facets, thereby restricting the crystal growth along the a- and b-axes, the octahedral $Ti(OH)_4$ fragments connect edge-sharing both longitudinally and laterally, with surface-edge adjustments leading to the formation of cuboidal TiO_2 nanocrystals. With repeated deionized water washing to slight alkalinity close to neutral hydrothermal environment, the OH^- gradually released from R-KTNWs, would preferentially attach to the anatase {100} facets and lowers the surface energy of the {100} facets, thereby restricting the crystal growth along the a- and b-axes. In this case no extra OH^-, the concentration of OH^- would gradually decrease with the reaction, the octahedral $Ti(OH)_4$ fragments connect edge-sharing along the equatorial plane and point-sharing longitudinally, eventually forming rod-like TiO_2 nanocrystals. R-KTNWs with acid washing followed by deionized water washing to subacidity close to neutral, part of $K_2Ti_3O_7$ nanowires were transformed into $H_2Ti_3O_7$ nanowires. The
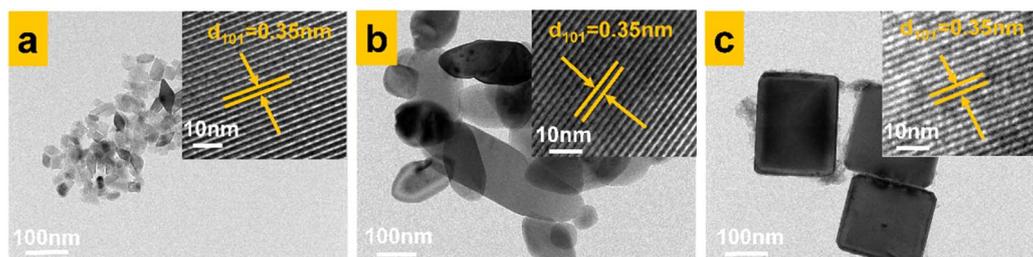

Fig. 2 TEM images of TiO_2 nanocrystals with different morphologies (a) TiO_2-R-H0, (b) TiO_2-R, (c) TiO_2-R-alk.

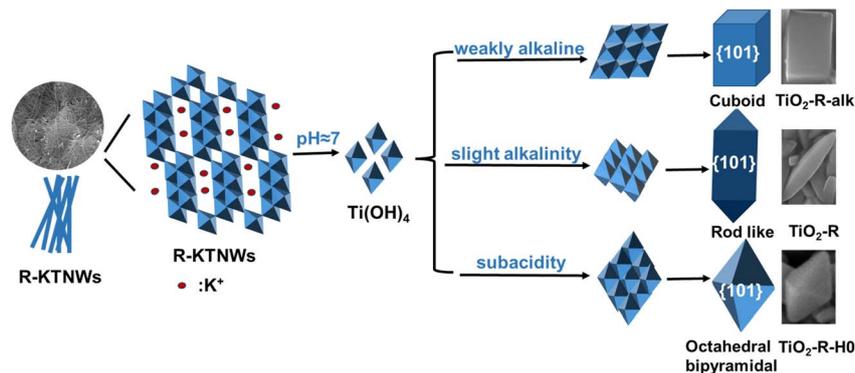© 2025 The Author(s). Published by the Royal Society of Chemistry

Fig. 3 The growth mechanism of TiO_2 nanocrystals with different morphologies synthesis during different hydrothermal condition.

splitting of the nanowires maybe along the {101} and {−101} facets and the growth of nanocrystals are accompanied by Ostwald ripening process, ultimately forming octahedral bipyramidal TiO_2 nanocrystals.[21]

Studies have shown that the morphology of TiO_2 nanocrystals is primarily governed by the growth rates along the [001] and [101] directions.[22] Under natural conditions, the surface energy of the {001} facet is higher (0.90 J m^{-2}), and the growth rate along the [001] direction is faster. According to the principle of minimum surface energy, the {101} crystal plane with lower surface energy (0.44 J m^{-2}) will eventually be exposed to minimize the surface energy.[23] By adjusting the pH of the solution through different washing methods, we obtained TiO_2 nanocrystals with varied morphologies, all contain {101} crystal plane, as shown in Fig. 2. This observation indicated that, the change of the pH of the hydrothermal solution will change the crystal growth mechanism to obtain TiO_2 with different morphologies, but will not change the characteristics of tending to expose low-energy {101} crystal facet to minimize the total surface energy of TiO_2 and make the system the most stable.

3.2 Effect of acid treatment of R-KTNWs on the morphology of TiO_2 nanocrystals

3.2.1 Morphological changes of R-KTNWs induced by acid treatment.
The above findings indicate that the properties of R-KTNWs play a crucial role in determining the morphology of subsequently synthesized TiO_2 nanocrystals. Acid washing of R-KTNWs results in the formation of bipyramidal TiO_2 nanocrystals with smaller particle sizes. Additionally, previous studies have reported that TiO_2 nanocrystals synthesized after exposing potassium titanate nanowires to an acidic environment for a certain period exhibit smaller particle sizes, which contributes to an increased specific surface area of TiO_2.[24] To further enhance the photocatalytic activity of TiO_2, we immersed the R-KTNWs precursor in HCl solution and stirred the mixture continuously at room temperature. This study aims to investigate the influence of acid treatment duration on the morphology, particle size, and photocatalytic activity of the resulting TiO_2 nanocrystals.

Fig. 4(a–c) show SEM images of R-KTNWs precursors subjected to different acid treatment durations. Fig. 4(a) and (b)

represent the SEM images of untreated R-KTNWs and those treated with acid for 7 hours, respectively. In both images, the R-KTNWs exhibit a uniform size distribution and clear, well-defined structures, with the nanowires intertwined. There are no significant morphological changes before and after acid treatment, indicating that a certain duration of acid treatment does not alter the macrostructure of the R-KTNWs. Liu *et al.* treated sodium titanate nanowires with 0.6 mol per L HCl for 1 h, HRTEM also showed that the morphology of the nanowires did not change before and after acid treatment, but the lattice fringe spacing changed from 0.81 nm to 0.78 nm after Na$^+$ were replaced by H$^+$.[25] As shown in Fig. 4(c), after further extending the acid treatment time to 48 h, although the appearance morphology still maintains the nanowire structure, the nanowires are significantly shortened and messy compared with the non-acid treatment, and some nanowires also appear to adhere to each other. If the acid treatment is prolonged to 72 h, the R-KTNWs nanowires are almost completely dissolved in the acid solution, indicating that the acid treatment duration should not be excessively long. Nakahira *et al.* also claimed that the symmetry of the Ti environment in TiO_2-derived titanate nanotubes has hardly changed with the post HCl treatment, local structures around Ti such as the coordination geometry in TiO_2-derived titanate nanotubes have changed with the acid treatment using HCl, and the excess acid treatment led to the disordering, and resulted in the change of the morphology.[26]

Therefore, it is essential to strictly control the preparation and washing processes of R-KTNWs in experiments to ensure that the surface properties of the nanowires remain consistent across batches and to minimize their impact on subsequent experiments. Fig. 4(d) shows the EDS spectra of R-KTNWs before and after 7 hours of acid treatment. The spectra reveal a significant reduction in the relative content of K$^+$ after acid treatment, with most K$^+$ ions being replaced by H$^+$ ions. The proportion of K$^+$ decreases from approximately 10% to about 3% after 7 hours of acid treatment. As discussed previously, after K$^+$ were replaced by H$^+$, both of the interlayer spacing and the thermal stability of the nanowires decreased.[26] The influence of the acid treatment duration of R-KTNWs precursors on the particle size, morphology, and photocatalytic activity of the TiO_2 nanocrystals were further investigated by TEM and photocatalytic activity test.
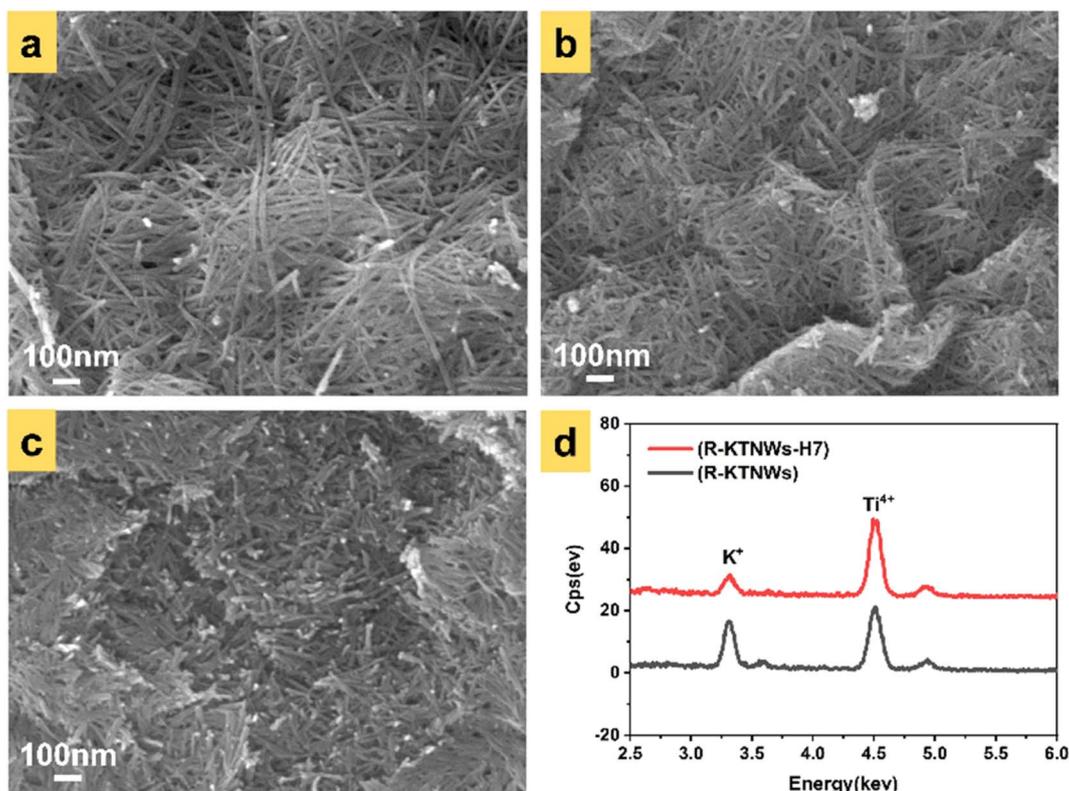
Fig. 4   SEM images of R–KTNWs nanowires treated with acid for different time, (a) 0 h, (b) 7 h, (c) 48 h, (d) EDS spectra.

3.2.2   The size and morphology changes of the synthesized TiO₂. Fig. 5 presents the TEM images of TiO₂ nanocrystals synthesized from R-KTNWs precursors subjected to different acid treatment durations. The results indicate that, similar to acid washing, acid treatment also could produce octahedral bipyramidal TiO₂ nanocrystals. The average particle size of different TiO₂ samples in TEM images was measured by Nano Measure software, the particle size distribution of TiO₂ nanocrystals synthesized after different acid treatment time for R-KTNWs precursors is shown in Fig. S1.† As shown in Fig. 5(a) and S1(a),† TiO₂ nanocrystals with a dominant octahedral bipyramidal morphology and an average particle size of approximately 42 nm were obtained after hydrothermal treatment of R-KTNWs acid-treated for 7 h. Extending the acid treatment to 24 h resulted in octahedral bipyramidal TiO₂

nanocrystals with a reduced average particle size of ~37.5 nm, accompanied by a small proportion of plate-like TiO₂ nanocrystals, as shown in Fig. 5(b) and S1(b).† For R-KTNWs acid-treated for 48 h, the resulting TiO₂ nanocrystals included bipyramidal structures along with a higher proportion of irregular plate-like morphologies, likely due to damage to the precursor structure. The average particle size of TiO₂ nanocrystals at this stage was approximately 37.2 nm, as shown in Fig. 5(c) and S1(c).†

3.2.3   Mechanism analysis of acid treatment of R-KTNWs to change the morphology of TiO₂. The acid treatment of the precursor transforms the morphology of the TiO₂ from rod-like to the typical bipyramidal structure, with particle size decreasing as the acid treatment duration increases. This indicates that acid treatment can effectively control the
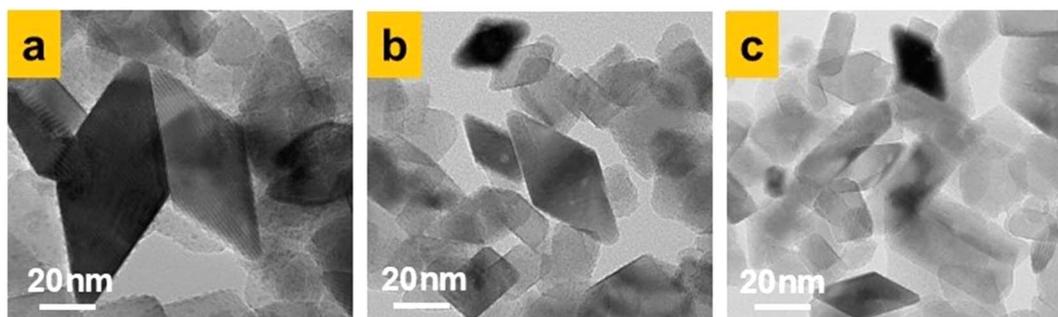

Fig. 5   TEM images of TiO₂ nanocrystals synthesized after acid treatment for different time, (a) TiO₂-R-H7, (b) TiO₂-R-H24, (c) TiO₂-R-H48.

morphology and particle size of TiO_2 nanocrystals, promoting the formation of bipyramidal TiO_2 nanocrystals. However, excessively long acid treatment durations are undesirable, as the proportion of bipyramidal TiO_2 structures decreases with prolonged treatment, leading to the emergence of other irregular morphologies. This indicates that acid treatment effectively controls the morphology and particle size of TiO_2 nanocrystals, promoting the formation of bipyramidal TiO_2 nanocrystals.

It can be concluded that the variation in K^+ content within potassium titanate nanowires is not the primary factor driving changes in TiO_2 morphology. Instead, the pH of the hydrothermal solution is the main determinant of the formation of bipyramidal TiO_2 nanocrystals. In acidic environments, TiO_2 nuclei grow into bipyramidal structures through point-sharing and edge-sharing mechanisms.[27] The reduction in particle size is attributed to the decrease in K^+ content caused by acid treatment, which reduces the interlayer spacing of potassium titanate and ultimately results in smaller TiO_2 nanocrystals.[28] Smaller particle sizes correspond to larger specific surface areas, which are beneficial for enhancing photocatalytic activity.[29] However, excessively long acid treatment durations can overly reduce K^+ content, compromise the stability of potassium titanate nanowires, and decrease the crystallinity of TiO_2 nanocrystals, leading to the formation of irregular morphologies.[30]

The mechanism of morphology and particle size changes in TiO_2 nanocrystal after acid treatment of R-KTNWs was illustrated in Fig. 6. During acid treatment, K^+ ions in R-KTNWs are gradually replaced by H^+ ions. With prolonged acid treatment, the structurally stable R-KTNWs undergoes protonation to form $H_2Ti_3O_7$. $H_2Ti_3O_7$ exhibits weak acidity and a negative zeta potential. During hydrothermal conversion, its negatively charged surface attracts H^+ ions from the reaction medium, resulting in the protonation of Ti–OH groups to form $Ti–OH_2^+$.[31] Two $Ti(OH)_4$ fragments then undergo rearrangement and dehydration to polymerize into TiO_2 crystal nucleus, which grow along the {101} plane.

This transition from $H_2Ti_3O_7$ to anatase TiO_2 nanocrystal involves the *in situ* dehydration and rearrangement of $Ti(OH)_4$ structural units and is thus considered a topochemical reaction, ultimately yielding octahedral bipyramidal TiO_2 nanocrystals.[31] The replacement of K^+ ions in R-KTNWs during this process reduces the interlayer spacing, which in turn decreases the particle size of the TiO_2 nanocrystals.

3.3 Photocatalytic activity of acid-treated TiO_2 nanocrystals

To explore the relationship between precursor acid treatment conditions and the photocatalytic activity of the synthesized TiO_2 nanocrystals, a series of TiO_2 nanocrystals were subjected to methylene blue (MB) photocatalytic degradation experiments. As illustrated in Fig. 7, TiO_2 nanocrystals prepared from acid-treated R-KTNWs precursors exhibited better photocatalytic activity than those prepared without acid treatment (TiO_2-R). However, as the acid treatment duration increased, the photocatalytic activity of the TiO_2 nanocrystals initially increased and then decreased. Among the samples, TiO_2-R-H7, synthesized from a precursor acid-treated for 7 hours, showed the fastest degradation rate of MB, with photocatalytic activity nearly 3 times and 5 times higher than that of the original anatase TiO_2 and TiO_2-R, respectively.

The enhanced photocatalytic activity can be attributed to the morphological and particle size changes of the TiO_2 nanocrystals after acid treatment. As previously analyzed, the acid treatment of R-KTNWs precursors transforms the morphology of the synthesized TiO_2 from nanorods to bipyramidal structures, with particle size decreasing from 303 nm to 42 nm or smaller. The improvement in TiO_2 crystallinity and the increase in specific surface area significantly enhance the photocatalytic activity of the TiO_2 nanocrystals. As show in Fig. 5, with the extension of acid treatment time to 24 h or even 48 h, although the particle size was further reduced to 37.2 nm, the proportion of octahedral bipyramidal TiO_2 structures decreases, and irregular morphologies emerge due to the excess acid treatment, resulting in a decline in photocatalytic activity. Additionally, acid treatment converts most of the Ti–O–K bonds on the surface of R-KTNWs into Ti–OH bonds, as H^+ replaces the larger K^+ ions. This substitution increases the number of surface oxygen vacancies, the hydroxyl group content, thereby enhancing the photocatalytic activity. However, with the excess acid treatment, the content of hydroxyl groups and oxygen vacancies decreases due to the continued action of the acid, leading to a reduction in photocatalytic activity.[32,33]

The oxygen vacancies of acid-treated TiO_2 nanocrystals were analyzed using EPR, and the results are shown in Fig. 8. Theoretically, within a certain range, a higher content of oxygen vacancies is beneficial for enhancing photocatalytic activity. However, excessive oxygen vacancies can act as recombination centers for photogenerated charge carriers, leading to a decline in photocatalytic activity of TiO_2.[34]

As shown in Fig. 8, no oxygen vacancies were detected in the original anatase TiO_2. The rod-like TiO_2-R, synthesized from untreated precursors, exhibited the highest oxygen vacancy content at $g = 2.003$. The bipyramidal TiO_2-R-H7, obtained after 7 hours of acid treatment, displayed a slightly lower oxygen vacancy peak intensity. The oxygen vacancy content further decreased in the TiO_2-R-H24 sample synthesized after 24 hours of acid
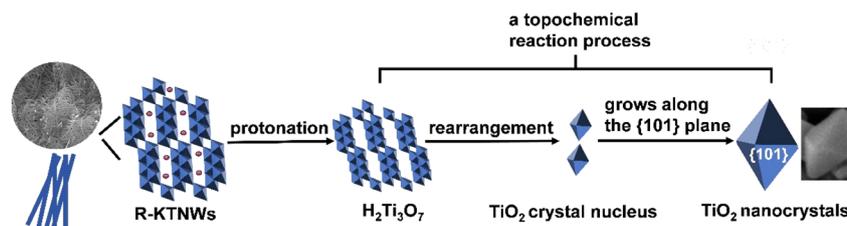

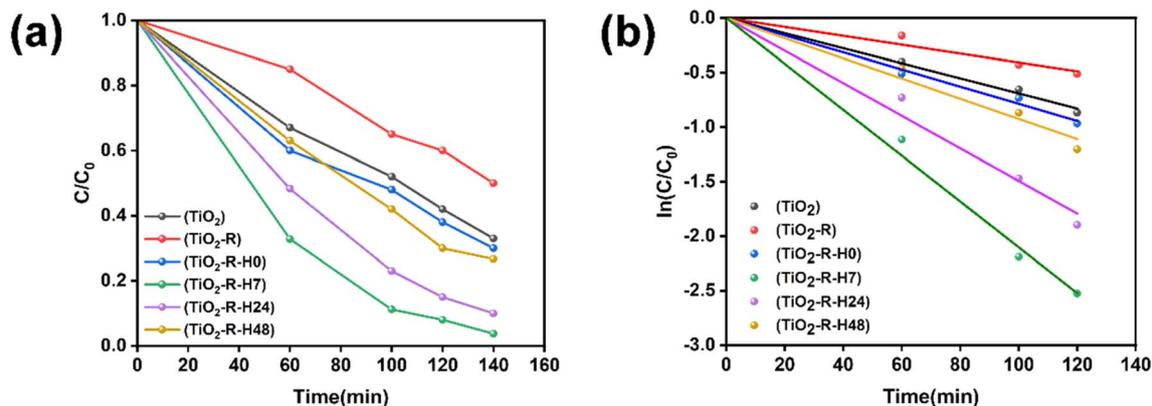**Fig. 6** The growth mechanism of TiO_2 nanocrystals after precursor acid treatment.

Fig. 7 Photocatalytic activity diagram of TiO$_2$ nanocrystals synthesized after precursor acid treatment (a) photocatalytic degradation diagram of MB, (b) photodegradation rate diagram.
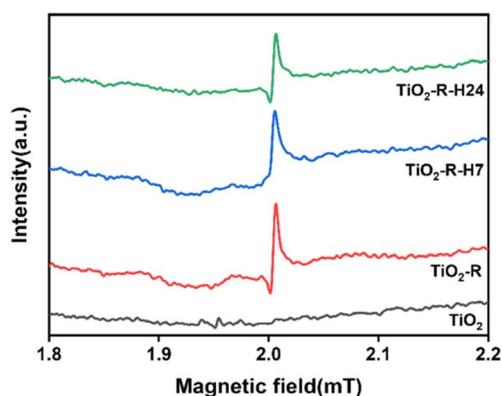

Fig. 8 Oxygen vacancy diagram of TiO$_2$ nanocrystals synthesized by acid treatment for different time.

treatment. These findings indicate that the synthesis method employed in this study effectively promotes the formation of oxygen vacancies in TiO$_2$. However, prolonged acid treatment of KTNWs will reduce the oxygen vacancy content in TiO$_2$.

From the photocatalytic activity results in Fig. 7, it can be observed that, despite the high oxygen vacancy content, the rod-like TiO$_2$-R nanocrystals exhibit relatively low photocatalytic activity due to their larger particle size. As the precursor acid treatment time increases, the oxygen vacancy content on the TiO$_2$ surface gradually decreases, and the crystallinity deteriorates, ultimately resulting in reduced photocatalytic activity. This demonstrates that the photocatalytic activity of TiO$_2$ is influenced by multiple factors, including particle size, morphology, and oxygen vacancy content. Moderate acid treatment of KTNWs precursors provides a stable approach for synthesizing bipyramidal TiO$_2$ nanocrystals with reduced particle size and increased surface oxygen vacancy content. This is one of the effective methods to enhance the photocatalytic activity of TiO$_2$.

3.4 Morphology of TiO$_2$ nanocrystals controlled by (NH$_4$)$_2$CO$_3$

Based on the previous work, this study employed (NH$_4$)$_2$CO$_3$ as a morphology-controlling agent to investigate whether exposing

highly active {001} crystal facets while maintaining small particle sizes can further enhance the photocatalytic activity of TiO$_2$. Fully washed and acid-treated 7 h R-KTNWs precursors were selected for subsequent crystal facet control experiments. By varying the concentration of the (NH$_4$)$_2$CO$_3$ solution during the hydrothermal process, the exposure ratio of the {001} crystal facets was controlled. The morphologies of the two groups of TiO$_2$ samples are shown in Fig. 9.

As shown in Fig. 9(a), using fully washed R-KTNWs as precursors, TiO$_2$-R samples without (NH$_4$)$_2$CO$_3$ were hydrothermally synthesized into rod-like TiO$_2$ nanocrystals with a length of 303 nm and a width of 103 nm. When varying concentrations of (NH$_4$)$_2$CO$_3$ morphology-controlling agents were introduced during hydrothermal synthesis using the same R-KTNWs precursors, truncated decahedral TiO$_2$ nanocrystals were obtained. Fig. 9(b–d) illustrate the morphologies of TiO$_2$-R-0.07, TiO$_2$-R-0.14, and TiO$_2$-R-0.28, corresponding to (NH$_4$)$_2$CO$_3$ concentrations of 0.07 mmol L^{-1}, 0.14 mmol L^{-1}, and 0.28 mmol L^{-1}, respectively. The average particle sizes of these samples were 68 nm, 98 nm, and 105 nm, respectively. Calculations showed that the proportion of exposed {001} facets was 7%, 11%, and 15%, respectively. As the proportion of {001} facets increased, the particle size of the TiO$_2$ nanocrystals also gradually increased. The study of Han *et al.* also shown the phenomenon that the particle size of TiO$_2$ nanocrystals increases with the increase of urea concentration.[35] In this work, the adsorption of NH$_4^+$ on the {001} facet reduced the surface energy, changed the crystal growth direction and finally exposed the {001} facet. It is speculated that the higher the concentration of (NH$_4$)$_2$CO$_3$, the more NH$_4^+$ adsorbed on the {001} plane, and the proportion of {001} plane also increased, which ultimately increased the particle size.

As shown in Fig. 9(e), when R-KTNWs acid-treated for 7 hours were used as precursors without the addition of (NH$_4$)$_2$CO$_3$, bipyramidal TiO$_2$ nanocrystals with an average particle size of approximately 42 nm were obtained. Compared to the rod-like TiO$_2$ shown in Fig. 9(a), the particle size was reduced by approximately 86%. When the acid-treated 7 h R-KTNWs were hydrothermally synthesized in (NH$_4$)$_2$CO$_3$ solutions with concentrations of 0.07 mmol L^{-1}, 0.14 mmol L^{-1}, and
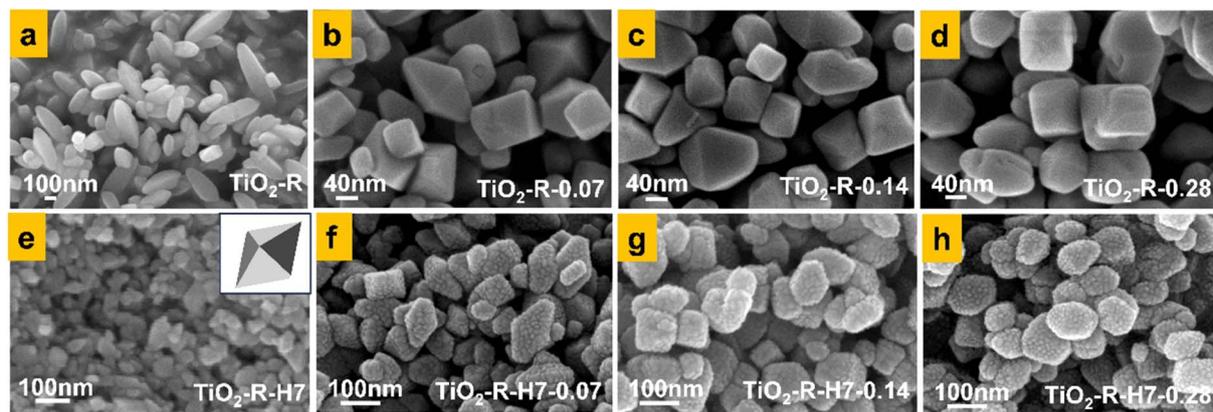
Fig. 9 SEM images of TiO$_2$ nanocrystals prepared under different conditions, (a) TiO$_2$-R, (b) TiO$_2$-R-0.07, (c) TiO$_2$-R-0.14, (d) TiO$_2$-R-0.28, (e) TiO$_2$-R-H7, (f) TiO$_2$-R-H7-0.07, (g) TiO$_2$-R-H7-0.14, (h) TiO$_2$-R-H7-0.28.

0.28 mmol L^{-1}, truncated decahedral TiO$_2$ nanocrystals exposing {001} facets were similarly obtained, as shown in Fig. 9(f–h). The proportions of exposed {001} facets were approximately 6%, 10%, and 12%, respectively, and the average particle sizes of the TiO$_2$ nanocrystals were about 71 nm, 85 nm, and 93 nm. The small particles observed on the TiO$_2$ particle surfaces are gold clusters for the SEM test.

These results demonstrate that the (NH$_4$)$_2$CO$_3$ morphology-controlling agent promotes the formation of {001} crystal facets, while the acid treatment of nanowire precursors significantly reduces the particle size of TiO$_2$ nanocrystals and increases their specific surface area.

To further confirm the presence of {001} facets in TiO$_2$, HRTEM characterization was performed on the TiO$_2$-R-0.14 sample. The results, shown in Fig. 10, reveal lattice fringes with a spacing of 0.35 nm, corresponding to the {101} crystal plane of TiO$_2$ nanocrystals, and a spacing of 0.24 nm, corresponding to the {001} crystal plane. These findings indicate that (NH$_4$)$_2$CO$_3$ effectively reduces the surface energy of the TiO$_2$ {001} facets, facilitating their exposure.[10]

We selected several typical samples of original TiO$_2$, TiO$_2$-R-0.14, TiO$_2$-R-H-0.07 for XRD detection, the results are shown in Fig. S2.† It can be seen from the figure that the diffraction peaks of TiO$_2$-R-0.14 and TiO$_2$-R-H-0.07 correspond to those of anatase TiO$_2$. It can be seen that pure anatase TiO$_2$ nanocrystals were prepared by crystal plane control in this work.

3.5 Photocatalytic activity of TiO$_2$ nanocrystals with exposed {001} facets

3.5.1 Effect of (NH$_4$)$_2$CO$_3$ on photocatalytic activity of non-acid treated series TiO$_2$ nanocrystals.
To investigate the effect of crystal facet engineering on the photocatalytic activity of TiO$_2$ nanocrystals, photocatalytic degradation experiments of MB were conducted under UV light irradiation. As shown in Fig. 11(a and b), TiO$_2$-R, synthesized by direct hydrothermal treatment of fully washed R-KTNWs without facet engineering, exhibited the weakest photocatalytic activity, followed by original anatase TiO$_2$. The photocatalytic activity of TiO$_2$ synthesized from fully washed R-KTNWs improved with increasing

concentrations of (NH$_4$)$_2$CO$_3$ but then declined beyond a certain concentration. The TiO$_2$-R-0.14 sample, synthesized at an (NH$_4$)$_2$CO$_3$ concentration of 0.14 mmol L^{-1}, showed the highest photocatalytic activity, with a degradation rate about 3.6 times that of the TiO$_2$-R sample and 2.6 times that of the original anatase TiO$_2$.

The low activity of the rod-like TiO$_2$-R sample can be attributed to its large particle size, with a length of 303 nm, 15.2 times larger than the particle size of the original anatase TiO$_2$. The improvement in photocatalytic activity upon introducing the (NH$_4$)$_2$CO$_3$ morphology-controlling agent is primarily due to the exposure of the high-energy {001} facets. Additionally, the formation of heterojunctions between the {101} and {001} facets also enhanced the separation efficiency of electron–hole pairs. This is because of preferential flow of photogenerated holes and electrons to the oxidative {001} facets and reductive {101} facets, on which oxidation and reduction occur respectively.[36] In particular, Maitani *et al.* demonstrated that the magnitude of electron transfer from anthracene derivatives to the {001} facet is 10 times larger than that to the {101} facets of TiO$_2$ nanocrystals.[37] This finding unambiguously suggests that the {001} facets are significantly more enriched with positively charged holes compared to the {101} facets, rendering the {001} facets more reactive for photooxidation processes. Thus, the coexistence of both the {001} facets (oxidation site) and {101} facets (reduction site) facilitate the prolonged separation of photogenerated electron–hole pairs. This spatial separation enhances the efficiency of TiO$_2$ nanocrystals in the photocatalytic degradation of MB. However, as shown in Fig. 9(d), when the concentration of (NH$_4$)$_2$CO$_3$ reached 0.28 mmol L^{-1}, the average particle size of TiO$_2$-R-0.14 sample increased to 105 nm and significant defects appeared on the surfaces of the TiO$_2$ nanocrystals, along with the emergence of many irregularly shaped particles. The increase of the particle size would decrease the specific surface area of the TiO$_2$ crystals, and the defects would act as recombination centers for electron–hole pairs, ultimately reducing the photocatalytic activity of the TiO$_2$ nanocrystals. This indicates that although the (NH$_4$)$_2$CO$_3$ morphology-controlling agent can promote the formation of high-energy
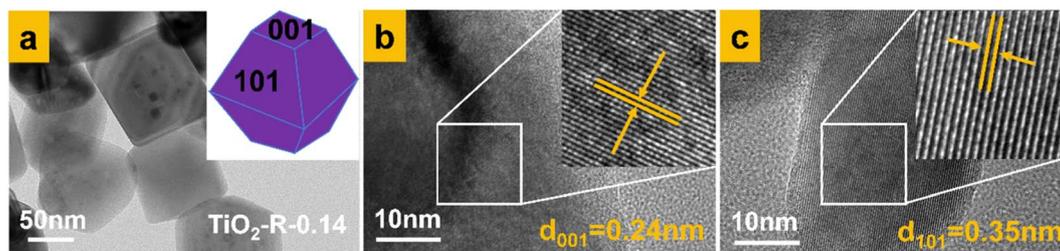
Fig. 10 TEM and HRTEM images of TiO_2-R-0.14 nanocrystals, (a) TEM image of TiO_2-R-0.14 nanocrystals, (b) {001} crystal plane partial enlarged detail, (c) {101} crystal plane partial enlarged detail.

{001} crystal facet of TiO_2, considering the comprehensive factors affecting the photocatalytic activity, the concentration of $(NH_4)_2CO_3$ in the synthesis process should not be excessively high.

The photocatalytic activity of samples with crystal facet engineering was higher than that of the original TiO_2 nanoparticles. Although the photocatalytic activity of the TiO_2-R-0.14 nanocrystals was about 2.6 times that of the original TiO_2 nanoparticles, their particle size was approximately 98 nm, which is about 4.9 times larger than the particle size of the original anatase TiO_2. This indicates that crystal facet engineering effectively enhances the photocatalytic activity of TiO_2, but excessively large particle size remains a limiting factor for further improvement. Therefore, it is necessary to further reduce the particle size while maintaining the benefits of crystal facet engineering.

3.5.2 Effect of $(NH_4)_2CO_3$ on photocatalytic activity of acid-treated series TiO_2 nanocrystals.

As shown in Fig. 9, compared with non-acid treatment, acid treatment of R-KTNWs followed by crystal facet engineering effectively reduces particle size. The photocatalytic activity of the resulting TiO_2 nanocrystals is shown in Fig. 12(a and b). From Fig. 12(b), it can be seen that TiO_2 nanocrystals synthesized after a 7 h acid treatment of R-KTNWs exhibit better photocatalytic activity compared to the original TiO_2 nanoparticles. The photocatalytic activities of the samples TiO_2-R-H7, TiO_2-R-H7-0.07, and TiO_2-R-H7-0.14, synthesized at different $(NH_4)_2CO_3$ concentrations, were about

2.9, 1.9, and 1.4 times that of anatase TiO_2, respectively. Among these, the TiO_2-R-H7 sample, synthesized without $(NH_4)_2CO_3$, exhibited the highest photocatalytic activity, with nearly complete degradation of MB after 120 min of UV irradiation, indicating that acid treatment enhances the photocatalytic activity of TiO_2 nanocrystals.

However, different from the series of samples without acid treatment, introducing $(NH_4)_2CO_3$ to synthesize TiO_2 nanocrystals from 7 h acid-treated R-KTNWs did not further enhance the photocatalytic activity. Instead, as the $(NH_4)_2CO_3$ concentration increased, the photocatalytic activity of the synthesized TiO_2 nanocrystals gradually decreased. Based on Fig. 9 SEM morphology and particle size analysis, this reduction in photocatalytic activity may be attributed to the lower proportion of {001} facets in the acid-treated samples, which limits the formation of crystal facet heterojunctions. Additionally, the increased particle size negatively impacts photocatalytic activity. The particle sizes of TiO_2-R-H7-0.07 and TiO_2-R-H7-0.14 were approximately 71 nm and 85 nm, respectively, which are about 1.7 and 2 times larger than that of the TiO_2-R-H7 sample.

3.5.3 The relationship between the concentration of $(NH_4)_2CO_3$ and the photocatalytic degradation rate constant of a series of TiO_2 nanocrystals.

To visually demonstrate the MB degradation activity of the TiO_2 samples, the relationship between photocatalytic degradation rate constants and $(NH_4)_2CO_3$ concentration was plotted. As shown in Fig. 13, the degradation rate constant of the original anatase TiO_2 was
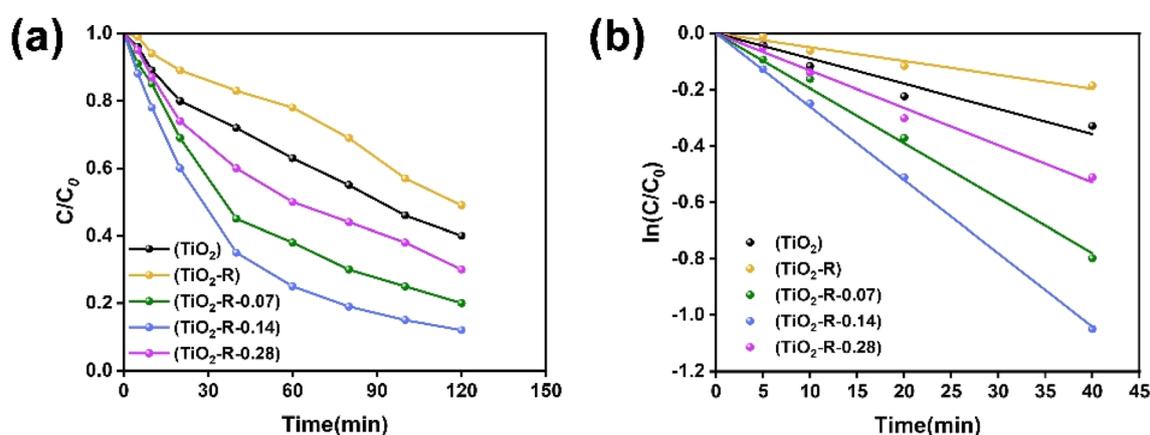

Fig. 11 Photocatalytic activity diagram of TiO_2 nanocrystals with exposed {001} crystal plane, (a) photocatalytic degradation of MB by synthesized TiO_2 without acid treatment, (b) photodegradation rate diagram.
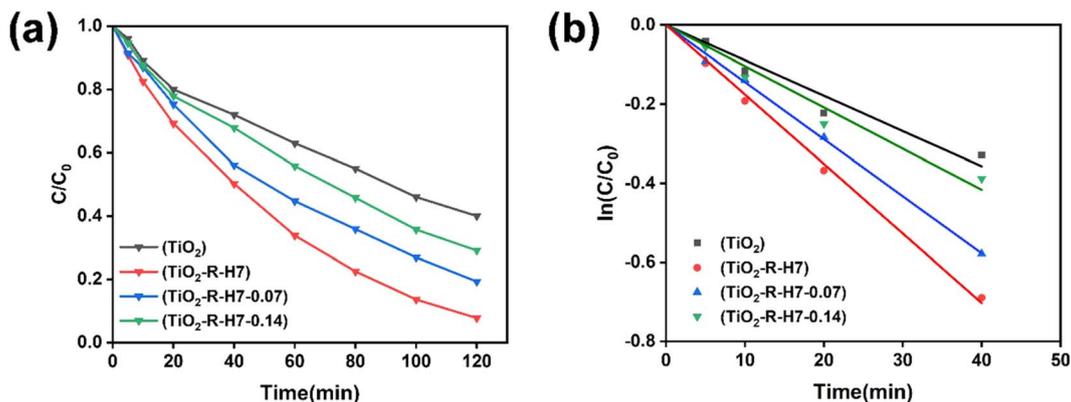
Fig. 12 Photocatalytic activity diagram of TiO_2 nanocrystals with exposed {001} crystal plane, (a) photocatalytic degradation of MB by synthesized TiO_2 with acid treatment, (b) photodegradation rate diagram.

0.0074. The rate constants for TiO_2-R, TiO_2-R-0.07, TiO_2-R-0.14, and TiO_2-R-0.28, prepared from fully washed R-KTNWs with crystal facet control, were 0.0054, 0.0144, 0.01959, and 0.01031, respectively. The most active sample, TiO_2-R-0.14, exhibited a rate constant about 2.6 times that of the original TiO_2.

For samples synthesized from R-KTNWs acid-treated for 7 hours, the rate constants of TiO_2-R-H7, TiO_2-R-H7-0.07, and TiO_2-R-H7-0.14 were 0.0213, 0.0137, and 0.0105, respectively, all of which were higher than those of the non-acid-treated series. Among these, TiO_2-R-H7 had the highest rate constant, approximately 2.9 times that of the original anatase TiO_2. These results indicate that TiO_2-R-H7, synthesized from acid-treated potassium titanate without the addition of $(NH_4)_2CO_3$, exhibited the highest photocatalytic activity. Adding $(NH_4)_2CO_3$ did not further enhance the activity.

From the SEM morphology images, it can be observed that the acid-treated samples exhibit a relatively low proportion of exposed {001} facets than no acid-treated samples at the same $(NH_4)_2CO_3$ concentration. Therefore, at this scale, changes in particle size have a greater impact on their photocatalytic

activity. This highlights that acid treatment of potassium titanate precursors could reduce the particle size of TiO_2 during crystal facet engineering, effectively enhancing the photocatalytic activity of TiO_2 nanocrystals. The acid-treated precursors exhibit surface acidity, which may influence subsequent crystal facet engineering. To further improve the photocatalytic activity of TiO_2 through crystal facet control, it is necessary to explore the optimal concentration of $(NH_4)_2CO_3$ as a morphology-controlling agent and investigate the structure–activity relationship between acid treatment and crystal facet engineering.

3.6 Spectral analysis of the synthesized TiO_2 nanocrystals

3.6.1 PL analysis. The separation and recombination of photogenerated electron–hole pairs in two series of TiO_2 nanocrystals, synthesized from precursors treated with 7 hours acid washing and fully water washing with crystal facet control, were investigated using photoluminescence (PL) spectroscopy. The results are shown in Fig. 14. The characteristic peak at 400 nm corresponds to the intrinsic bandgap emission of TiO_2 due to electron–hole recombination, while other peaks may result from oxygen vacancies or other radical excitations.[38] Theoretically, lower peak intensities indicate higher electron–hole separation efficiency.[39]

As shown in Fig. 14(a), the PL peak intensity of fully washed, non-acid-treated TiO_2 nanocrystals after crystal facet control initially decreases and then increases with increasing $(NH_4)_2CO_3$ concentration. The TiO_2-R-0.14 sample, synthesized with 0.14 mmol per L $(NH_4)_2CO_3$, exhibited the lowest PL peak intensity, indicating the lowest electron–hole recombination rate and the highest photocatalytic activity. This trend is consistent with the photocatalytic activity trend shown in Fig. 11(a).

Fig. 14(b) shows that when R-KTNWs acid-treated for 7 hours are subjected to crystal facet control, the PL intensities of TiO_2-R-H7, TiO_2-R-H7-0.07, and TiO_2-R-H7-0.14 are all lower than those of the original TiO_2 nanoparticles. However, as the $(NH_4)_2CO_3$ concentration increases, the PL peak intensity
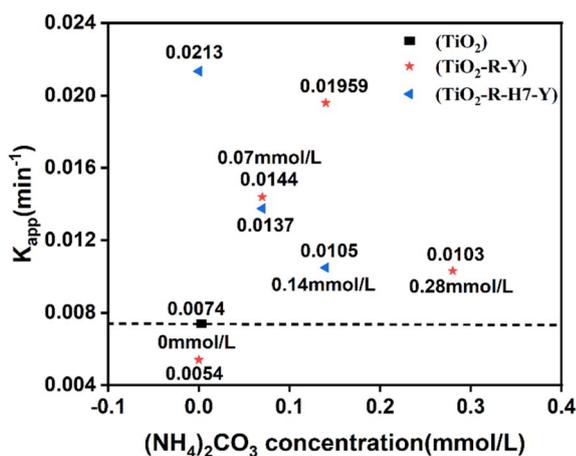

Fig. 13 The relationship between the concentration of $(NH_4)_2CO_3$ and the photocatalytic degradation rate constant of a series of TiO_2 nanocrystals.
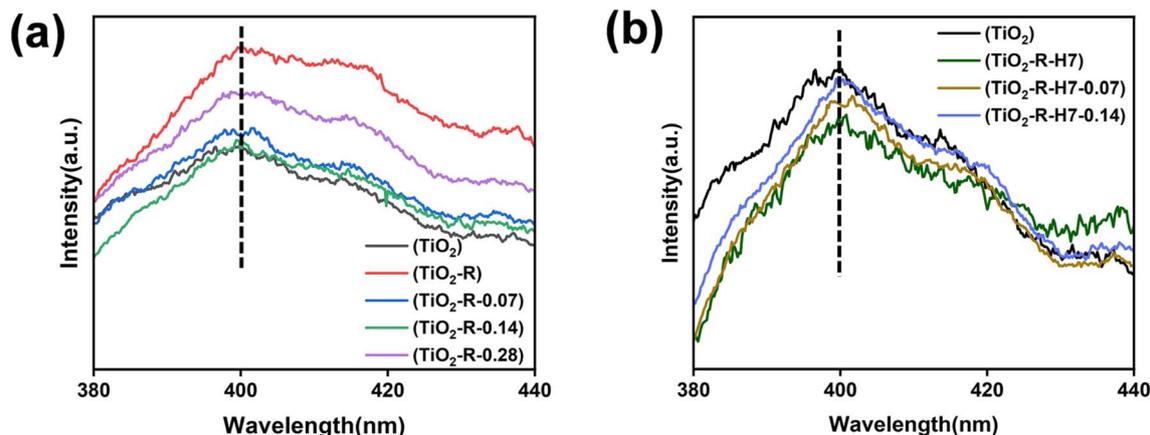
Fig. 14 Photoluminescence spectra of facet-controlled TiO_2 nanocrystals (a) synthesized TiO_2 without acid treatment, (b) synthesized TiO_2 with acid treatment.

gradually increases, corresponding to higher electron–hole recombination rates and weaker photocatalytic activity.

A comparison of the results for the 7 h acid-treated and non-acid-treated series reveals that all acid-treated samples exhibit lower PL peak intensities than their non-acid-treated counterparts, indicating that acid treatment effectively promotes carrier separation. Among these, the bipyramidal TiO_2-R-H7 sample, synthesized from 7 h acid-treated potassium titanate without $(NH_4)_2CO_3$, demonstrated the highest electron–hole separation efficiency and the strongest photocatalytic activity. This PL result aligns with the photocatalytic activity tests.

3.6.2 UV-vis analysis. The optical response range of different series of facet-controlled TiO_2 nanocrystals was analyzed using UV-visible diffuse reflectance spectroscopy, as shown in Fig. 15. It indicates that, compared to the original anatase TiO_2, the synthesized TiO_2 samples in this study exhibit stronger absorption intensity in the range of 400–650 nm, suggesting an expanded light absorption range.

The bandgap values were determined by drawing tangents at the steepest descent points of the absorption curves,[40] as shown in Fig. S3.† The original TiO_2 had a bandgap of 2.8 eV, while the bandgap values for the fully washed facet-controlled TiO_2-R series (TiO_2-R, TiO_2-R-0.07, TiO_2-R-0.14, TiO_2-R-0.28) were 2.75 eV, 2.68 eV, 2.6 eV, and 2.7 eV, respectively. After 7 hours of acid treatment, the bandgap values for the crystal-facet-engineered TiO_2–H7 series (TiO_2-R-H7, TiO_2-R-H7-0.07, TiO_2-R-H7-0.14) were 2.52 eV, 2.77 eV, and 2.74 eV, respectively.

For the fully washed R-KTNWs precursor, the bandgap of the crystal-facet-engineered TiO_2 decreased and then increased with the rise in $(NH_4)_2CO_3$ concentration, with TiO_2-R-0.14 exhibiting the smallest bandgap of 2.6 eV. Similarly, for the 7 h acid-treated R-KTNWs precursor, the bandgap of the TiO_2–H7 series also decreased and then increased with $(NH_4)_2CO_3$ concentration. The TiO_2-R-H7 sample, synthesized without $(NH_4)_2CO_3$, had the smallest bandgap of 2.52 eV.

The UV-visible diffuse reflectance trends align with the photocatalytic activity trends shown in Fig. 11 and 12. Both acid treatment and crystal facet engineering caused a redshift in the

light absorption edge of TiO_2, with the TiO_2-R-H7 sample exhibiting the largest redshift. This sample also demonstrated the highest electron–hole separation efficiency and the strongest corresponding photocatalytic activity.

3.6.3 EPR analysis. EPR analysis was conducted to investigate oxygen vacancies and further explain the trends in photocatalytic activity for the TiO_2 samples. An appropriate amount of oxygen vacancies can enhance the photocatalytic activity of TiO_2.[41] As illustrated in Fig. 16(a), no significant oxygen vacancy characteristic peaks were detected for the original TiO_2. However, distinct oxygen vacancy peaks were observed for the TiO_2-R and TiO_2-R-0.14 samples synthesized from fully washed R-KTNWs precursors. Among these, TiO_2-R-0.14, which exhibited the strongest photocatalytic activity in this series, also showed higher oxygen vacancy peak intensity.

The oxygen vacancy intensities for the acid-treated precursor series are shown in Fig. 16(b). The TiO_2-R-H7 sample, synthesized without $(NH_4)_2CO_3$, displayed relatively high oxygen vacancy peak intensity. In contrast, the TiO_2-R-H7-0.07 and TiO_2-R-H7-0.14 samples, synthesized with the addition of $(NH_4)_2CO_3$, showed significantly reduced oxygen vacancy intensities. It is speculated that the decline in photocatalytic activity for this series with increasing $(NH_4)_2CO_3$ concentration is not only related to the increase in TiO_2 nanocrystal particle size but also potentially to the decrease in oxygen vacancy content.

Based on the oxygen vacancy analysis, it can be concluded that moderate acid treatment of potassium titanate nanowire precursors enables the stable synthesis of small-sized bipyramidal TiO_2 nanocrystals while maintaining a sufficient level of oxygen vacancies. This effectively enhances the photocatalytic activity of TiO_2.

3.7 Stable synthesis route of TiO_2 nanocrystal photocatalysts with different morphologies

Highly active TiO_2 nanocrystal photocatalyst can be synthesized by controlling the crystal facet derived from KTNWs nanowire precursor. But discrepancies in the size and morphology of TiO_2
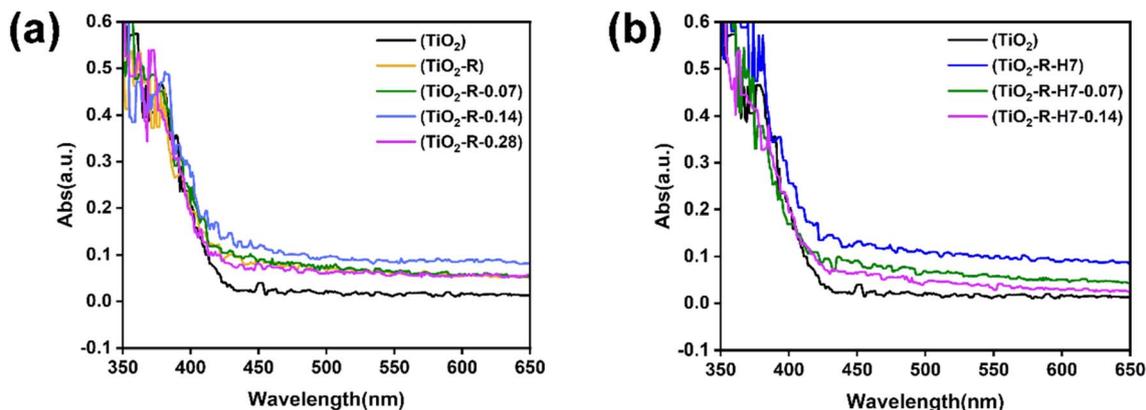
Fig. 15 UV-vis diffuse reflectance spectra of TiO$_2$ nanocrystals synthesized under different conditions, (a) TiO$_2$ synthesized without acid treatment, (b) TiO$_2$ synthesized after 7 h acid treatment.

nanocrystals synthesized using similar methods by different researchers highlight the need to explore the key factors influencing the morphology of TiO$_2$ nanocrystal. As show in Fig. 17, this study explored key factors influencing TiO$_2$ nanocrystal morphology using KTNWs as precursors.

We found that subtle changes in the pH of the hydrothermal solution played a critical role in controlling the morphology of TiO$_2$ nanocrystals. The transformation of commercial TiO$_2$ to R-KTNWs occurs in a strongly alkaline hydrothermal environment. It is difficult to achieve a completely neutral product through simple deionized water washing. Although washing steps were standardized, the difference in washing time and water dosage would also cause the difference in the surface acidity and alkalinity of the R-KTNWs precursor, which would affect the pH environment of the subsequent hydrothermal process, thereby influencing the growth direction of TiO$_2$ nuclei. We have realized the controllable synthesis of TiO$_2$ nanocrystals by simply adjusting the R-KTNWs precursor washing method, including deionized water washing resulting in weakly alkaline conditions, repeated deionized water washing to slight alkalinity close to neutral, and acid washing followed by deionized water washing to subacidity close to neutral, and cuboidal, rod-like, and octahedral bipyramidal

TiO$_2$ nanocrystals could be obtained, respectively. In the above several synthesis methods, acid treatment could stabilize the octahedral bipyramidal morphology of the TiO$_2$ nanocrystal, and with the extension of acid treatment time, the particle size can be reduced. In this work, the TiO$_2$-R-H7 sample synthesized after acid treatment of R-KTNWs for 7 h can stably obtain a uniform octahedral bipyramid structure with an average particle size of 42 nm, showing the best photocatalytic degradation of MB activity. By varying the concentration of the (NH$_4$)$_2$CO$_3$ morphology control agent during the hydrothermal process, the exposure ratio of the TiO$_2$ {001} crystal facets could be controlled. Exposing the highly active {001} facets of TiO$_2$ could form a heterojunction of {001} and {101} facets. The electrons tend to transfer to the {101} facets, and the holes tend to transfer to the {001} facets, which promotes the spatial separation of electrons and holes, thereby improving the photocatalytic activity of TiO$_2$ nanocrystals.[42] However, in this work, after the combination of acid treatment and crystal facet regulation, the exposure of {001} facet did not further improve the photocatalytic activity of TiO$_2$ due to the increase of particle size and insufficient exposure of {001} facet. The synergistic effect between acid treatment and crystal facet regulation needs to be further explored.
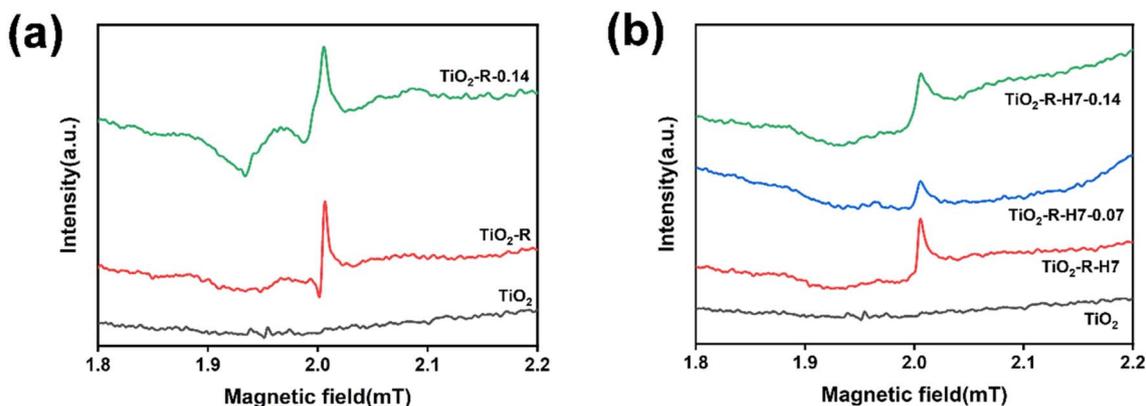

Fig. 16 Oxygen vacancy detection of facet-controlled TiO$_2$ nanocrystals synthesized under different conditions, (a) no acid treatment, (b) acid treatment for 7 h.
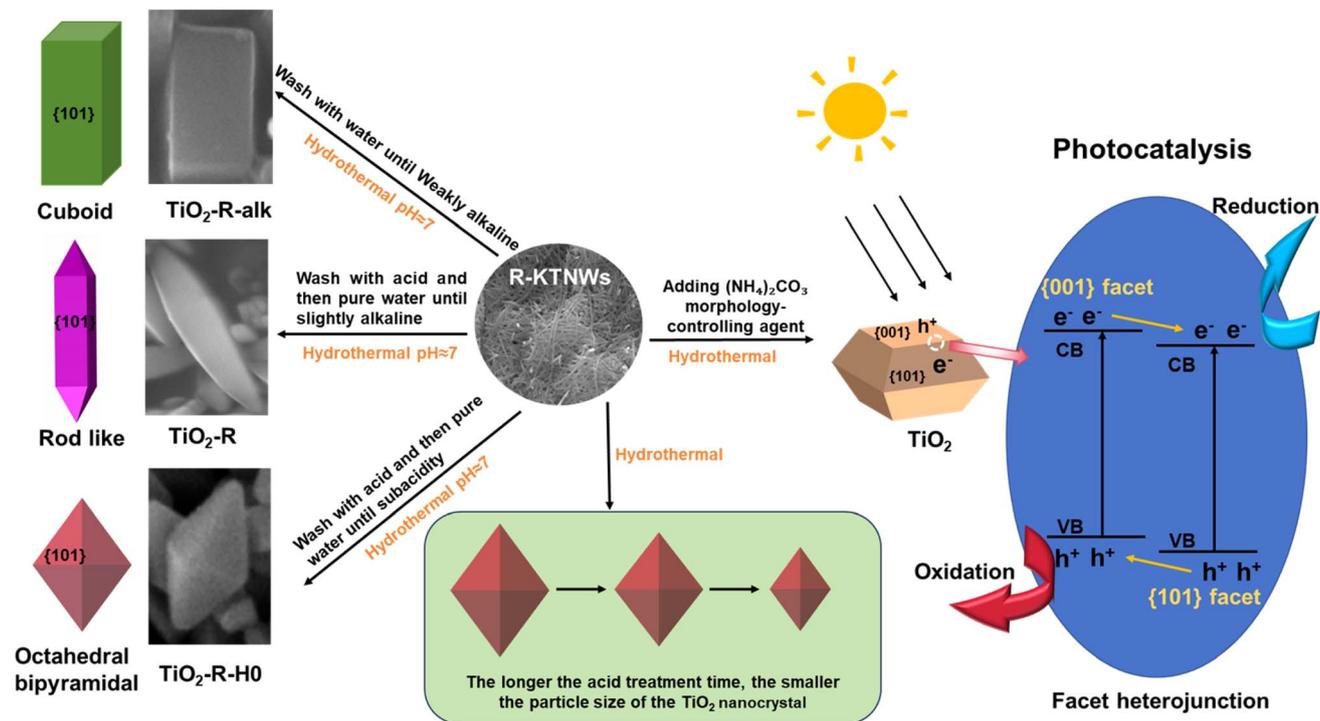
Fig. 17 Stable synthesis route of TiO_2 nanocrystal photocatalysts with different morphologies.

4. Conclusions

This study demonstrates that the morphology and photocatalytic activity of TiO_2 nanocrystals can be effectively controlled by adjusting the washing and acid treatment of R-KTNWs. Different washing methods for precursors synthesized under alkaline conditions lead to varying pH environments in the subsequent hydrothermal solutions, thereby influencing the growth direction of TiO_2 nuclei. A weakly alkaline hydrothermal solution produced cuboidal TiO_2 nanocrystals, a slight alkalinity near-neutral solution yielded rod-like TiO_2 nanocrystals, and a subacidity near-neutral solution resulted in octahedral bipyramidal TiO_2 nanocrystals. Acid treatment could reduce particle size and stabilize octahedral bipyramidal TiO_2 synthesis was considered as the best synthesis method in this work. By controlling the acid treatment duration, it was found that the reduction in K^+ content would decrease the interlayer spacing of R-KTNWs, leading to smaller TiO_2 particle sizes. However, prolonged acid treatment would reduce structural stability, crystallinity, and photocatalytic performance.

TiO_2-R-H7, synthesized from precursors acid-treated for 7 hours shown the best photocatalytic activity, exhibited a particle size reduction of 86% that of TiO_2-R and a photocatalytic activity nearly 5 times and 3 times that of TiO_2-R and original TiO_2, respectively. Introducing $(NH_4)_2CO_3$ morphology-controlling agent to synthesis {001} facet exposed TiO_2, but did not surpass the photocatalytic activity of TiO_2-R-H7 due to increased particle size, reduced oxygen vacancies, and insufficient {001} facet exposure. Further improvement of the photocatalytic activity of TiO_2 nanocrystals requires in-depth exploration of the structure–activity relationship between acid treatment and crystal facet engineering. This study provides insights into the growth mechanisms of TiO_2 morphologies and highlights acid treatment as a strategy to reduce particle size and enhance photocatalytic activity, offering guidance for designing high-performance photocatalytic materials.

Data availability

The data supporting the findings of this study are available within the article and its ESI.† Additional data are available from the corresponding author and the data have not been submitted to any public repository.

Author contributions

Meng Chai: writing – original draft, writing – review & editing, methodology, investigation, data curation. Bo Yuan: writing – review & editing, conceptualization. Yao Ban: investigation, methodology, data curation. Jing Guo: writing – original draft, writing – review & editing, resources, project administration, funding acquisition, conceptualization. Huifang Lou: investigation. Hongyuan Kang: investigation. Qiaoling Zhang: supervision. Zhiwei Liu: funding acquisition, writing – review & editing. Dongming Zhang: funding acquisition, writing – review & editing.

Conflicts of interest

All the authors have approved the manuscript and agree with submission to your esteemed journal and there are no conflict of interest exits in the submission of this manuscript.

Acknowledgements

References

1 Y. Du, X. Niu, J. He, L. Liu, Y. Liu, C. Chen, X. Yang and Q. Feng, *ACS Omega*, 2020, **5**, 14147–14156.

2 N. Parsafard, R. Abedi and H. Moodi, *RSC Adv.*, 2024, **14**, 19984–19995.

3 L.-Y. Zhang, Y.-L. Han, M. Liu and S.-L. Deng, *RSC Adv.*, 2023, **13**, 16797–16814.

4 R. Katal, S. Masudy-Panah, M. Tanhaei, M. H. D. A. Farahani and H. Jiangyong, *Chem. Eng. J.*, 2020, **384**, 123384.

5 L. Liu, Y. Du, X. Niu, W. Li, J. Li, X. Yang and Q. Feng, *ChemistrySelect*, 2018, **3**, 9953–9959.

6 J. Wang, B. Liu and K. Nakata, *Chin. J. Catal.*, 2019, **40**, 403–412.

7 C. Yao, X. Wang, W. Zhao, T. Li, Y. He, X. Ran and L. Guo, *J. Alloys Compd.*, 2020, **846**, 156335.

8 K. Zhu, H. Gao, G. Hu and Z. Shi, *J. Supercrit. Fluids*, 2013, **83**, 28–34.

9 X. Han, X. Wang, S. Xie, Q. Kuang, J. Ouyang, Z. Xie and L. Zheng, *RSC Adv.*, 2012, **2**, 3251.

10 Y. Du, X. Niu, K. Hou, X. He and C. Zhang, *Catalysts*, 2022, **12**, 232.

11 D. K. Chacko, A. A. Madhavan, T. A. Arun, S. Thomas, G. S. Anjusree, T. G. Deepak, A. Balakrishnan, K. R. V. Subramanian, N. Sivakumar, S. V. Nair and A. S. Nair, *RSC Adv.*, 2013, **3**, 24858.

12 P. V. Viet, B. T. Phan, L. V. Hieu and C. M. Thi, *J. Nanosci. Nanotechnol.*, 2015, **15**, 5202–5206.

13 J. Xiong and L. He, *J. Exp. Nanosci.*, 2017, **12**, 384–393.

14 Z. Wei, E. Kowalska, K. Wang, C. Colbeau-Justin and B. Ohtani, *Catal. Today*, 2017, **280**, 29–36.

15 Z. Wei, E. Kowalska, J. Verrett, C. Colbeau-Justin, H. Remita and B. Ohtani, *Nanoscale*, 2015, **7**, 12392–12404.

16 Y. Du, Q. Feng, C. Chen, Y. Tanaka and X. Yang, *ACS Appl. Mater. Interfaces*, 2014, **6**, 16007–16019.

17 C. Chen, L. Xu, G. A. Sewvandi, T. Kusunose, Y. Tanaka, S. Nakanishi and Q. Feng, *Cryst. Growth Des.*, 2014, **14**, 5801–5811.

18 J. Li and D. Xu, *Chem. Commun.*, 2010, **46**, 2301.

19 A. S. Barnard and L. A. Curtiss, *Nano Lett.*, 2005, **5**, 1261–1266.

20 A. S. Barnard, P. Zapol and L. A. Curtiss, *Surf. Sci.*, 2005, **582**, 173–188.

21 L. Liu, Y. Du, X. Niu, W. Li, J. Li, X. Yang and Q. Feng, *ChemistrySelect*, 2018, **3**, 9953–9959.

22 C. H. Cho, M. H. Han, D. H. Kim and D. K. Kim, *Mater. Chem. Phys.*, 2005, **92**, 104–111.

23 S. Li, L. Ruan, S. Wang, Z. Wang, Z. Ren and G. Han, *J. Mater. Sci. Technol.*, 2020, **46**, 139–144.

24 J. Wang, H. Li, H. Wang, K. Huang, G. Sun, S. Yin and T. Sato, *Res. Chem. Intermed.*, 2011, **37**, 165–175.

25 B. Liu, J. E. Boercker and E. S. Aydil, *Nanotechnology*, 2008, **19**, 505604.

26 A. Nakahira, T. Kubo and C. Numako, *ACS Appl. Mater. Interfaces*, 2010, **2**, 2611–2616.

27 Y. Yu and D. Xu, *Appl. Catal. B Environ.*, 2007, **73**, 166–171.

28 T. Gupta, Samriti, J. Cho and J. Prakash, *Mater. Today Chem.*, 2021, **20**, 100428.

29 M. Humayun, F. Raziq, A. Khan and W. Luo, *Green Chem. Lett. Rev.*, 2018, **11**, 86–102.

30 J. Xiong and L. He, *J. Exp. Nanosci.*, 2017, **12**, 384–393.

31 M. Sluban and P. Umek, *J. Phys. Chem. C*, 2019, **123**, 23747–23757.

32 L. K. Dhandole, M. A. Mahadik, S.-G. Kim, H.-S. Chung, Y.-S. Seo, M. Cho, J. H. Ryu and J. S. Jang, *ACS Appl. Mater. Interfaces*, 2017, **9**, 23602–23613.

33 C. Lv, X. Lan, F. Li, L. Wang, L. Xiao, C. Wang, J. Shi and S. Yu, *Catal. Sci. Technol.*, 2020, **10**(3), 690–699.

34 W. Wang, C.-H. Lu, Y.-R. Ni, J.-B. Song, M.-X. Su and Z.-Z. Xu, *Catal. Commun.*, 2012, **22**, 19–23.

35 X. Han, X. Wang, S. Xie, Q. Kuang, J. Ouyang, Z. Xie and L. Zheng, *RSC Adv.*, 2012, **2**, 3251.

36 N. Roy, Y. Sohn and D. Pradhan, *ACS Nano*, 2013, **7**, 2532–2540.

37 M. M. Maitani, K. Tanaka, D. Mochizuki and Y. Wada, *J. Phys. Chem. Lett.*, 2011, **2**, 2655–2659.

38 E. P. Estévez Ruiz, J. L. Lago and S. P. Thirumuruganandham, *Materials*, 2023, **16**, 3076.

39 J. Zhu, S. Zhu, X. Kong, Y. Liang, Z. Li, S. Wu, S. Luo, C. Chang and Z. Cui, *ACS Appl. Nano Mater.*, 2020, **3**, 10349–10359.

40 X. Zhang, H. Zhang, H. Zhang, L. Peng and S. Huang, *New J. Chem.*, 2024, **48**, 17458–17464.

41 F. Li, G. Liu, F. Liu, J. Wu and S. Yang, *J. Hazard. Mater.*, 2023, **452**, 131237.

42 A. K. R. Police, S. V. P. Vattikuti, Y.-J. Baik and B. Chan, *Ceram. Int.*, 2019, **45**, 2178–2184.